Materials Horizons

ROYAL SOCIETY OF CHEMISTRY

COMMUNICATION

View Article Online
View Journal

Cite this: DOI: 10.1039/d3mh00988b

Received 29th June 2023,
Accepted 20th July 2023

DOI: 10.1039/d3mh00988b

rsc.li/materials-horizons

Solid state solvation: a fresh view†

Brunella Bardi, ‡[a] Davide Giavazzi, ‡[a] Elena Ferrari, [a] Alessandro Iagatti, [bc] Mariangela Di Donato, [cd] D. K. Andrea Phan Huu, [a] Francesco Di Maiolo, [a] Cristina Sissa, [a] Matteo Masino, [a] Andrea Lapini *[ac] and Anna Painelli *[a]

The design of efficient organic electronic devices, including OLEDs, OPVs, luminescent solar concentrators, *etc.*, relies on the optimization of relevant materials, often constituted by an active (functional) dye embedded in a matrix. Understanding solid state solvation (SSS), *i.e.* how the properties of the active dye are affected by the matrix, is therefore an issue of fundamental and technological relevance. Here an extensive experimental and theoretical investigation is presented shedding light on this, somewhat controversial, topic. The spectral properties of the dye at equilibrium, *i.e.* absorption and Raman spectra, are not affected by the matrix dynamics. Reliable estimates of the matrix polarity are then obtained from an analysis of the micro-Raman spectra of polar dyes. Specifically, to establish a reliable polarity scale, the spectra of DCM or NR dispersed in amorphous matrices are compared with the spectra of the same dyes in liquid solvents with known polarity. On the other hand, steady-state emission spectra obtained in solid matrices depend in a highly non-trivial way on the matrix polarity and its dynamics. An extensive experimental and theoretical analysis of the time-resolved emission spectra of NR in a very large time window (15 fs–15 ns) allows us to validate this dye as a good probe of the dielectric dynamics of the surrounding medium. We provide a first assessment of the relaxation dynamics of two matrices (mCBPCN and DPEPO) of interest for OLED application, unambiguously demonstrating that the matrix readjusts for at least 15 ns after the dye photoexcitation.

New concepts

OPV and OLED efficiency crucially relies on careful optimization of the active dye in its local surrounding, making solid state solvation a powerful, but so far poorly understood and exploited, materials design tool. We propose an original and easy approach to reliably estimate the static dielectric properties of an amorphous matrix from the Raman spectra of dispersed dyes. Unprecedented information on the dielectric dynamics of mCBPCN and DPEPO matrices, commonly used in OLEDs, is obtained from the emission spectra of a carefully selected dye in a time window ranging from ~15 fs to ~15 ns. The dielectric relaxation, responsible for a sizable red-shift of the emission, is characterized by matrix-dependent timescales, extracted *via* a detailed theoretical analysis. The proposed approach to static and dynamic dielectric behaviour is easily applicable to any amorphous material. These results shed new light on the emission properties of dyes in amorphous matrices, an issue of enormous interest for OLED production.

1 Introduction

Organic electronics relies on molecular functional materials whose properties are exploited in several devices including organic LEDs (OLEDs), organic photovoltaics (OPVs), luminescent solar concentrators, photodetectors *etc.*[1,2] Organic-based devices are low-cost, are composed of abundant elements and offer an opportunity for easy recycling, while exploiting the enormous tunability of molecular properties provided by synthetic approaches. The interaction between functional molecules and the local environment, if properly mastered, offers a powerful tool to optimize the material for a specific application. Indeed, the unique properties of molecules of interest for advanced applications – large absorption or emission features in the visible-near IR regions, large non-linear optical responses, multistability, charge transport *etc.* – are related to the presence of extended π-conjugated backbones which are responsible for the large (hyper)polarizability of functional molecules, and hence for their large responsivity to any perturbation due to the local environment.

Solvatochromism, the solvent dependence of the spectral properties of a dye, is the easiest demonstration of the responsivity of π-conjugated molecules to the local environment. Solvatochromism is well understood: the first models date back to the work of Liptay[3] and more recently Reichardt[4] and

[a] *Dept. Chemistry, Life Science and Environmental Sustainability, University of Parma, Parco Area delle Scienze 17/A, 43124 Parma, Italy. E-mail: andrea.lapini@unipr.it, anna.painelli@unipr.it*
[b] *CNR-INO (Istituto Nazionaledi Ottica), Largo Fermi 6, 50125 Firenze, Italy*
[c] *LENS (European Laboratory for Non-Linear Spectroscopy), Via N. Carrara 1, 50019, Sesto Fiorentino, FI, Italy*
[d] *ICCOM-CNR, via Madonna del Piano 10, I-50019 Sesto Fiorentino, FI, Italy*

† Electronic supplementary information (ESI) available. See DOI: https://doi.org/10.1039/d3mh00988b

‡ These authors contributed equally to this work.

Ratner,[5] while the Lippert–Mataga plots,[6] relating the absorption and emission frequencies of a dye to the dielectric properties of the solvent, are well established tools used to extract useful information on the permanent dipole moment of polar molecules in the ground and excited states. Several computational strategies have been devised to address solvation phenomena that either rely on a continuum dielectric model[7–10] for the solvent or on atomistic descriptions.[11] Both strategies should be considered with care for the electronic component of solvation,[12,13] yet they offer a reliable approach to polar solvation.

Solid state solvation (SSS) is much less investigated and understood. Its relevance to OLEDs was recognized early by Forrest and coworkers who exploited the large dependence of the emission color of a dye on the polarity of the environment to tune the color of phosphorescent OLEDs[14] and to create white-OLEDs.[15] Green *et al.*[16] exploited SSS in solar light concentrators, tuning the dielectric properties of the polymeric matrix with the addition of camphor (a small polar dopant) to optimize the absorption properties of a dye dispersed in the matrix and hence the efficiency of the solar concentrator. Doping organic matrices with camphor,[17] ethylene glycols[18] or other small molecules[19] was also proposed to improve the efficiency of organic solar cells, with limited success.[20] The importance of matrix effects, and hence of SSS, in the third generation of OLEDs was recognized early on.[21] In these devices, non-emissive triplet states are harvested *via* a mechanism called thermally activated delayed fluorescence (TADF) which relies on a tiny energy gap between the lowest energy singlet and triplet states and on well-balanced mixing between charge transfer (CT) and local excited triplet states.[22,23] The delicate TADF mechanism is largely affected by SSS,[24–27] indeed a smart matrix approach has been proposed to optimize the device performance *via* concurrent optimization of the dye inside the matrix.[28] Several experimental and theoretical works were devoted to disentangling the subtle effects of the matrix in TADF-OLEDs: on one side the dielectric properties of the matrix are important, but for sure its rigidity plays a role, altering the conformation of the emitter.[29,30]

SSS has been discussed so far with reference to fluorescence, paying very little, if any, attention to environmental effects on absorption and vibrational spectra. However, when focusing on fluorescence, a delicate issue must be considered that makes SSS more complex and difficult to deal with than liquid solvation. The relevant degrees of freedom of liquid (low-viscosity) solvents relax in the first few picoseconds after the solute photoexcitation,[27,31,32] so that fluorescence (typically in the nanosecond timescale) occurs from the solute experiencing a fully relaxed environment. In frozen glassy solvents, the environment is very rigid and its relaxation is fully hindered.[33] But in polymeric or in small molecule matrices at room temperature the situation is much less clear cut. Of course the molecules cannot freely tumble inside a matrix, however the matrix is not fully frozen. As discussed in polymeric matrices,[34] polar groups can rotate around C–C bonds and other groups may librate in timescales that are strongly dependent on the environment.

The dynamical behavior of the matrix is of enormous relevance to control the physics of actual devices.[20,30,35,36] As an example, camphor is often added to matrices to increase their dielectric constant.[16,17,29,37] However, as demonstrated by a careful analysis,[38] the camphor molecules readjust quickly inside the matrix, with typical relaxation times in the picosend time window, so that the matrix behaves like a liquid polar environment. Experimental data on the dielectric response of small molecule matrices are scarce[39] and even less is known about their dynamical behavior, most results relying on molecular dynamics simulations.[35,40]

Here we present a combined experimental and theoretical study of several matrices, typically adopted in OLED fabrication, addressing their dielectric properties and dynamical behavior. The approach, relying on donor–acceptor dyes exploited as microscopic polarity sensors, is easily generalized to other types of matrices or media, offering a useful characterization tool to exploit SSS towards optimized optoelectronic devices.

2 Results and discussion

2.1 SSS and steady-state spectra

Polar dyes are good molecular polarity probes, indeed a well-known polarity scale of liquid solvents relies on their solvatochromism.[4] Here we exploit two polar dyes, 4-(dicyanomethylene)-2-methyl-6-(4-dimethylaminostyryl)-4*H*-pyran (DCM) and Nile Red (NR) in Fig. 1, whose photophysics is well understood.[41,42] When a polar dye enters a liquid or solid medium, the medium polarizes in response to the dye dipole moment (for the sake of simplicity, we limit attention to dipolar terms, the leading terms in the solute–solvent interaction) generating a local electric field, dubbed as the reaction field. Two contributions to the reaction field must be considered, a contribution related to the electronic polarizability of the medium molecules, and a contribution related to the conformational/rotational degrees of freedom of the medium. The first contribution is traced back to the medium refractive index at optical frequencies. Since the refractive index is roughly invariant in different organic media, to a first approximation, its contribution to the solvatochromism can be disregarded.[43] To be more specific, the medium polarizability largely and non-trivially affects the photophysics of a dye when going from

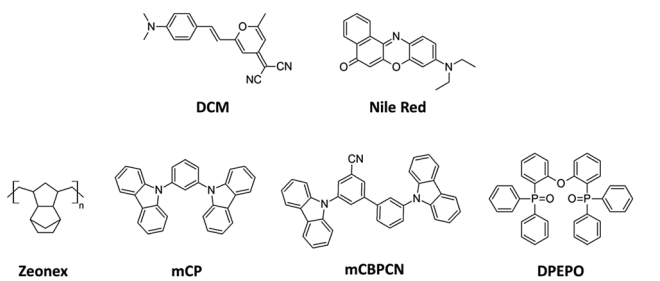

Fig. 1 The two polar dyes used as polarity sensors in this study and the chemical structures of the matrices of interest.

gas phase to an organic medium (the refractive index changing from 1 to ~1.4),[26] but the effect is roughly the same in all common organic media, so that the large variation of spectral properties in different solvents/matrices can be safely ascribed to the second contribution. In the liquid phase, the solvent molecules are free to tumble: in the presence of a polar dye, they reorient to generate at the solute location a reaction field F_R proportional to the solute dipole moment $\langle\hat{\mu}\rangle$[3,4,43]:

$$F_R = r\langle\hat{\mu}\rangle \quad (1)$$

where r increases with the solvent polarity. In solid matrices, the molecular units or the polymeric fragments are not moving freely, however, during the formation of the matrix, it is likely that polar molecules and/or polar groups arrange themselves around a polar dye generating again a reaction field proportional to the dipole moment of the dye. Once again, one expects that matrices containing polar molecules or polar groups will generate a sizable reaction field.

We are now in the position to understand the absorption and Raman spectra of DCM and NR dissolved in solvents of increasing polarity, from carbon tetrachloride (CCl_4) to dimethylsulfoxide (DMSO) and dispersed in matrices of different polarity, as shown in Fig. 2 and 3. Both dyes have a polar ground state, with a permanent dipole moment μ_g smaller than the very large excited state dipole moment μ_e associated with the CT nature of the excited state.[41] The absorption transition is a vertical process, occurring while the slow degrees of freedom stay frozen and $F_R = r\mu_g$. The energy of the excited state is then lowered, due to the interaction with the environment by $-F_R\mu_e = -r\mu_g\mu_e$. The energy of the ground state is also lowered but by a smaller amount $-F_R\mu_g = -r\mu_g\mu_g$, so that the absorption transition moves to the red upon increasing the solvent polarity (as schematically shown in Fig. 4):

$$\hbar\omega_{abs} = \hbar\omega^0_{abs} - r\mu_g(\mu_e - \mu_g) \quad (2)$$

where ω^0_{abs} is the absorption frequency in non-polar media. The absorption spectra in Fig. 2 and 3 clearly point to a solvent polarity that increases from CCl_4 to $CHCl_3$ to DMF and DMSO.

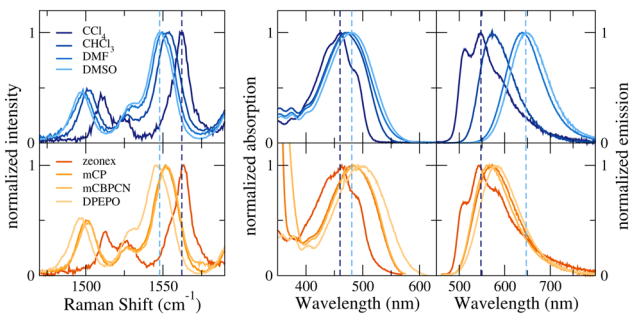

Fig. 2 DCM steady-state spectra. Top panels show spectra collected in liquid solvents; bottom panels show spectra collected in matrices. From left to right we show Raman spectra (complete spectra are reported in the ESI,† Fig. S2), absorption and fluorescence spectra. Absorption spectra in matrices are measured as fluorescence excitation spectra. The vertical dashed lines show, as a guide for the eye, the positions of the band maxima measured in CCl_4 and DMSO.

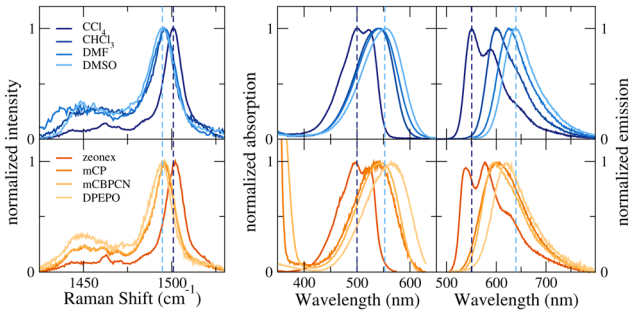

Fig. 3 NR steady-state spectra. Top panels show spectra collected in liquid solvents; bottom panels show spectra collected in matrices. From left to right we show Raman spectra (complete spectra are reported in the ESI,† Fig. S3), absorption and fluorescence spectra. Absorption spectra in matrices are measured as fluorescence excitation spectra. The vertical dashed lines show, as a guide for the eye, the positions of the band maxima measured in CCl_4 and DMSO.

The absorption spectra of NR show a larger solvatochromism than DCM, in line with NR having a larger permament dipole moment than DCM.[41,42] We underline that molecules with a very small permanent dipole moment $\mu_g \sim 0$, like *e.g.* most of TADF dyes, show marginal absorption solvatochromism. Finally, the progressive broadening of the absorption band with increasing solvent polarity is ascribed to the inhomogenous broadening induced by thermal disorder on the reaction field.[41,43] The narrow absorption bands with partially resolved vibronic structures seen in non-polar solvents should not be ascribed to the local excited state: even absorption bands due to CT transitions stay well resolved in non-polar solvents.[41,42,44,45] The comparison between the absorption spectra of the two dyes in different environments defines a polarity scale for the matrices: Zeonex is non polar, since the two dyes in Zeonex have similar spectra as in CCl_4, mCP and mCBPCN have similar polarity as DMSO, while DPEPO is even more polar than DMSO.

Vibrational solvatochromism, recently proposed as a powerful tool to monitor the local medium polarity,[46] has been extensively investigated in polar donor–acceptor dyes.[47–49] In short, the polarity of donor–acceptor dyes slightly increases with the medium polarity, and as a result, coupled vibrational modes move to the red (in the hypothesis of linear electron–vibration coupling). The non-resonant Raman spectra of DCM in Fig. 2 are more sensitive to the polarity than those of NR (Fig. 3), but for both systems, they support the same polarity scale as absorption spectra. Once again, Zeonex behaves like CCl_4, mCP and mCBPCN have similar polarity, being slightly less polar than DMSO, and DPEPO is as polar as or possibly slightly more polar than DMSO. We underline that, much like absorption, the Raman bands also broaden in polar media.[49]

The consistency of the information obtained from the Raman and absorption spectra makes us confident that both approaches offer reliable polarity estimates. Raman definitely is the best choice: even if it requires slightly larger dye concentrations, being a microscopic technique, it allows us to control the sample homogeneity and aggregation phenomena. Collecting absorption spectra from films is instead tricky. Indeed we

collected excitation spectra, but, as discussed in detail in Section 1.1 of the ESI,† extreme care has to be taken to work with very tiny dye concentrations and/or very thin films in order to minimize autoabsorption phenomena.

Understanding matrix effects on fluorescence spectra is delicate and deserves attention. Upon excitation to the CT state, the permanent dipole moment of the dyes of interest considerably increases. In liquid solvents, just a few picoseconds are needed for the solvent molecules to rearrange in response to the new molecular polarity. Steady-state fluorescence, typically in the nanosecond timescale, therefore occurs from a state where the excited dye is experiencing a reaction electric field $F_R = r\mu_e$. Along the same line that leads us to eqn (2), we can estimate the progressive red shift of the fluorescence band with the solvent polarity as (*cf.* Fig. 4):

$$\hbar\omega_{fluo} = \hbar\omega^0_{fluo} - r\mu_e(\mu_e - \mu_g) \quad (3)$$

where ω^0_{fluo} is the fluorescence frequency in non-polar media. Since our dyes have $\mu_e > \mu_g$, the solvatochromism is more pronounced in emission than in absorption. But again, for liquid solvents, the expected polarity scale is recovered, with the polarity increasing from CCl_4 to $CHCl_3$, DMF and DMSO.

However, if we look at the fluorescence spectra collected in solid matrices (*cf.* bottom panels of Fig. 2 and 3), we get a surprise: Zeonex, a non-polar matrix, behaves like CCl_4, as expected, but the other matrices look much less polar than they are in absorption. As the most striking example, Raman and absorption spectra suggest that DPEPO is as polar as or possibly slightly more polar than DMSO; but in emission DPEPO looks much less polar than DMSO. This is a clear indication that the matrix cannot fully readjust in response to the dye photoexcitation in the time-window of relevance to fluorescence. On the other hand, in the same timescale, the matrix is not fully rigid, as demonstrated by the sizable Stokes shifts observed in polar matrices. To understand SSS in fluorescence spectra, a time-resolved analysis is in order.

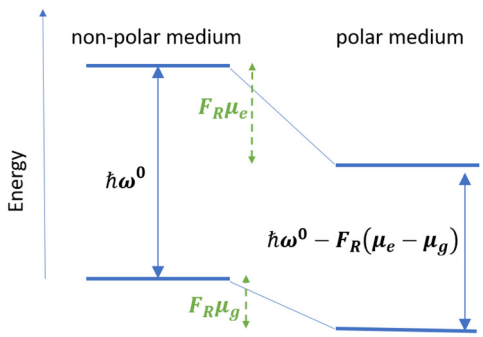

Fig. 4 A sketch of polar solvation effects on transition energies. The concept is the same for absorption and steady-state fluorescence spectra (ω^0 represents either the absorption or fluorescence energy of the dye in a non-polar environment): the energy of the excited and of the ground state is lowered by an amount $F_R\mu_e$ and $F_R\mu_g$, respectively so that the transition energy is lowered by $F_R(\mu_e - \mu_g)$. For absorption processes, $F_r = r\mu_g$, in either liquid or solid matrices. As for steady-state fluorescence, in liquid solvents $F_r = r\mu_e$, with the same solvent-specific r value as in absorption. In solid matrices the picture for steady-state fluorescence is more complex, as discussed in the text.

2.2 Fluorescence solvatochromism: a time-resolved study

Fig. 5 shows time resolved emission spectra (TRES) collected in the 1–15 nanosecond timescale (time correlated single photon counting, TCSPC, technique, see Section 3.4) for DCM and NR dispersed in Zeonex (Fig. S4, ESI† shows results for other matrices). In this non-polar (or very weakly polar) matrix, we do not expect any spectral evolution driven by the solvent rearrangement. Indeed the TRES of NR in Zeonex show a negligible time-dependence. The situation is completely different for DCM, whose emission spectra redshift by ~50 nm in the analyzed time-window. DCM has a flexible molecular structure and, at variance with NR, it is expected to undergo a geometrical relaxation that, inside the matrix, apparently occurs in the nanosecond timescale. Since we are interested in the characterization of the matrix dynamics, we discard DCM for the subsequent study. DCM is a good and reliable polarity probe as long as we are interested in the equilibrium polarity of the matrix, as tested by absorption and Raman spectra, but its flexibility makes it an unreliable probe for the dielectric dynamics of the matrix. To study the matrix relaxation we then exploit NR, a solvatochromic dye with a fairly rigid structure.

To better characterize the behavior of the matrices, we measured pump–probe spectra of NR dissolved in $CHCl_3$ and DMF solvents and in the non-polar Zeonex matrix and two polar mCBPCN and DPEPO matrices. Specifically, Fig. 6 shows (with a positive sign) the stimulated emission signal (additional data in the ESI,† Section 2.2). Pump–probe spectra, acquired with the US-pp setup (see Section 3.5), exploit a broad-band pump pulse and a broad-band probe pulse. As a result of the short pulses adopted, coherent oscillations are observed at early times, superimposed to the transient absorption signal (Fig. 6, upper panels) due to NR molecular vibrations. The time evolution of NR emission measured in amorphous matrices is strikingly different than in liquid solvents. In liquid solvents, the dynamics of the system is completed in ~10–15 ps for $CHCl_3$ solutions and ~1 ps for DMF solutions, in line with relevant solvent longitudinal relaxation times 2.8 and 0.91 ps, respectively.[32] In the two matrices instead, a progressive red-shift is seen that is not

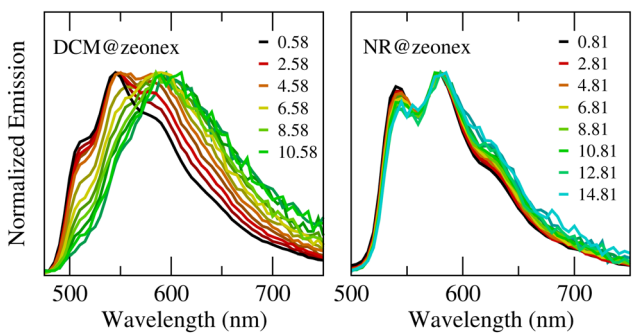

Fig. 5 Time resolved emission spectra of DCM and NR in Zeonex. Time units: ns. Data for other matrices are shown in Fig. S4 (ESI†).

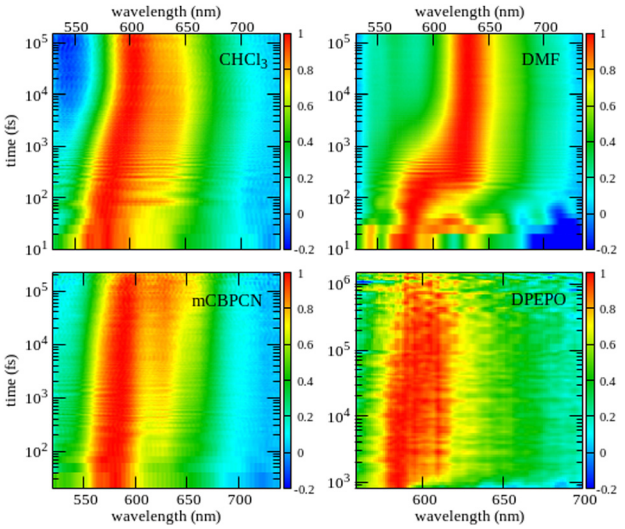

Fig. 6 Stimulated emission signal (positive sign) measured with the US-pp (see Section 3.5) pump–probe set up for NR in liquid solvents (top) and in matrices (bottom).

completed in the accessible time window (220 ps for mCBPCN and 1.5 ns for DPEPO in Fig. 6).

Fig. 7 summarizes the information from time-resolved measurements in the whole accessible spectral window. Specifically, in the upper panel we show for NR in mCBPCN the temporal evolution of the maximum of the NR stimulated emission band measured by pump–probe (US-pp, see Section 3.5) as well as the maximum of NR fluorescence spectra (TCSPC, see Section 3.4). In the lower panel the same information is reported for NR in DPEPO, together with pump–probe data obtained with the LR-pp setup (see Section 3.5). A very clear evolution of the maximum of the fluorescence band is seen that for both matrices extends up to the longest time accessible, ~15 ns. Indeed, the emission signal from NR (intrinsic lifetime ~4 ns) is too weak to be collected at longer times. To the best of our knowledge, reliable polarity sensors with distinctively longer lifetimes are not available. Phosphorescence signals live longer, but phosphorescence solvatochromism is poorly understood, and the simulation of the spectra is hindered by the weak emission signals. TADF dyes are solvatochromic and could allow us to follow fluorescence up to the μs window. However, TADF dyes typically undergo important conformational rearrangements upon photoexcitation[44,50] and/or are prone to conformational disorder,[29,30] so that disentangling the spectral shifts genuinely due to the dielectric relaxation from those due to the conformational degrees of freedom is hardly possible.

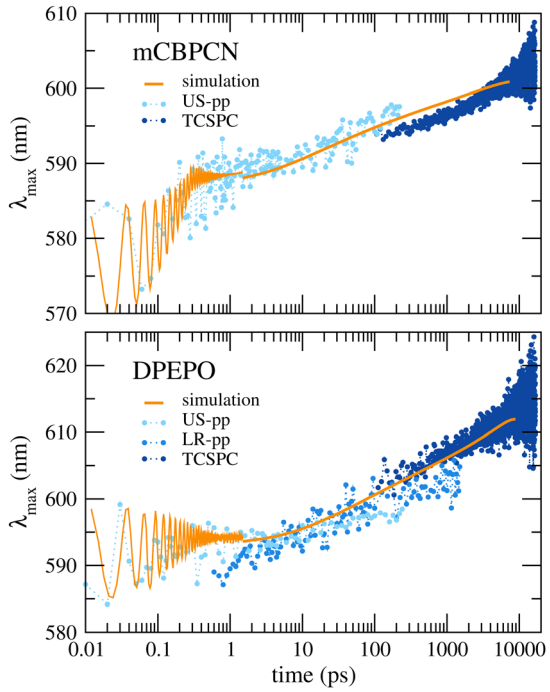

Fig. 7 Time evolution of the maximum of NR emission spectrum: bluish dots refer to experimental data collected with different techniques (as per the legend), and the orange line shows simulated results (molecular parameters in Table 1, matrix relaxation time, as discussed in the text). For better comparison, simulated spectra are red shifted by 2.5 nm for DPEPO (bottom panel) and by 6 nm for mCBP-CN (top panel).

To further confirm that the spectral diffusion observed in the 0.1 ps–15 ns interval in Fig. 7 is due to the relaxation of the matrix around the photoexcited dye, we have repeated the pump–probe experiment for NR in mCBPCN and DPEPO matrices at 77 K. At this temperature, the matrix relaxation is hindered and, as shown in Fig. S10 (ESI†), the spectral diffusion is virtually absent. We underline that our experimental results, definitely proving a rearrangement of the matrices that extends well into the ns timescale, contrast sharply with recent results from molecular dynamics simulation, where the matrix relaxation is observed in the ps timescale.[35]

2.3 Modeling NR in liquid solvents

The low energy photophysics of DCM and NR is well described in terms of an essential state model (ESM) that only accounts for two electronic states, corresponding to the neutral and zwitterionic molecular structures, coupled to a single effective vibration. The model was validated against steady-state linear and non-linear optical spectra of several donor–acceptor dyes and their aggregates.[41,42,47,51,52] For the sake of clarity, the model is summarized in the ESI,† here we underline that the steady-state absorption and fluorescence spectra of each dye and their evolution with the solvent polarity can be reproduced with good accuracy in terms of 4 molecular parameters, reported in Table 1, plus the solvent relaxation energy, a parameter that increases with the solvent polarity. Simulated steady-state absorption, fluorescence and vibrational spectra of NR (Fig. 8) compare well with the experiment (Fig. 3), confirming the reliability of the model and of its parametrization (simulated steady-state spectra of DCM are shown in Fig. S11, ESI†). Indeed the model captures well the complex evolution with the solvent polarity of the frequencies and band shapes of the absorption, fluorescence and vibrational spectra, only adjusting the solvent relaxation energy. Simulated vibrational spectra only account for a single vibrational mode, yet we can

Table 1 Molecular model parameters in eV for Nile Red and DCM. $2z_0$ measures the energy difference between the zwitterionic and neutral states, τ is the matrix elements that mixes the two states, and ε_v and ω_v are the vibrational relaxation energy and the vibrational frequency, respectively (see the ESI for more details)

	z_0	τ	ε_v	$\hbar\omega_v$
Nile Red	0.88	0.95	0.33	0.14
DCM	1.14	0.88	0.456	0.172

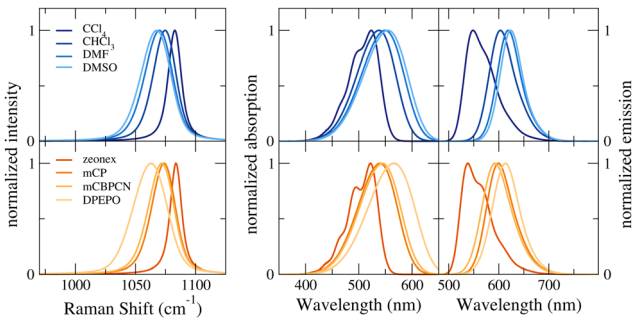

Fig. 8 NR calculated steady-state spectra. The top panels show simulated spectra in liquid solvents. The molecular parameters are listed in Table 1, and the solvent relaxation energies are set for all simulations to ε_{or} = 0.13, 0.47, 0.62, 0.68 eV for CCl_4, $CHCl_3$, DMF and DMSO, respectively. The bottom panels show the simulated spectra in matrices. Raman and absorption spectra are simulated setting the (total) solvent relaxation energy to ε_{or} = 0.08, 0.50, 0.56, 0.79 eV for Zeonex, mCP, mCBPCN and DPEPO, respectively. For the fluorescence spectra the relaxation energy is partitioned for each matrix into a static component set to ε_{or}^{st} = 0.0, 0.10, 0.28, 0.40 eV for Zeonex, mCP, mCBPCN and DPEPO, respectively and a dynamical component set, for the same matrices, to ε_{or}^{dyn} = 0.08, 0.4, 0.28, 0.39 eV. Of course the sum of the two components amounts to the total relaxation energy used for the absorption and Raman spectra. From left to right we show Raman, absorption and fluorescence spectra.

simulate the progressive red-shift and broadening of the vibrational band upon increasing the solvent polarity.

The time evolution of emission spectra is related to the concurrent relaxation of the photoexcited molecule and surrounding solvent. To address this complex phenomenon we exploit a strategy originally proposed to address energy transfer in solution.[53] Specifically, to account for the relaxation of the photoexcited dye we couple the vibrational coordinate of the dye to a thermal bath of harmonic oscillators.[54,55] As discussed in the ESI,† we adopt the Redfield approach and assume a constant spectral density for the bath degrees of freedom, so that a single parameter γ enters the definition of the molecular relaxation process, that we set to γ = 5 ps^{-1}. Finally, the relaxation of the solvent, that enters the model as a classical overdamped coordinate, is described by the Smoluchowsky equation.[53,56] The only parameter needed to describe the solvent relaxation is the longitudinal relaxation time, τ_l whose value is taken from the literature (see the ESI† for additional details).[32]

The color maps in the top panels of Fig. 9 show the time-resolved emission spectra calculated for NR dissolved in $CHCl_3$ and DMF. The agreement with experiment (Fig. 6) is impressive,

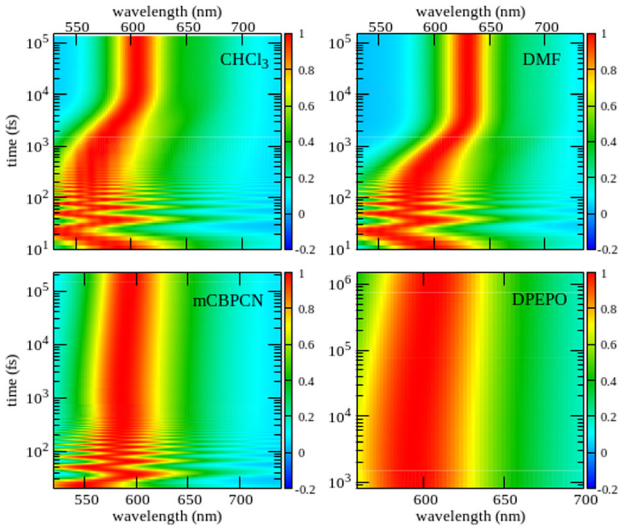

Fig. 9 Simulated time-resolved emission spectra of NR in different environments. Molecular parameters are listed in Table 1. The top panels refer to liquid solvents, $CHCl_3$ and DMF, whose longitudinal relaxation times are set to the literature values, τ_l = 2.8 and 0.91 ps, respectively. The bottom panels refer to mCBPCN and DPEPO matrices. As discussed in the text, a time-dependent relaxation time is introduced to simulate the matrix dynamics.

the main discrepancy being observed in the very early time. Indeed within the first few hundredths of fs the calculated spectra show very clear signatures related to coherent vibrational oscillations. These features are much less prominent in the experimental spectra. This minor discrepancy is traced back to the main approximation of the molecular model that accounts for a single effective vibrational mode coupled to the electronic degrees of freedom. In the actual molecule, several vibrations with different frequencies are coupled to the electronic system, somewhat suppressing the signal due to coherent oscillations.

2.4 Modeling NR in amorphous matrices

The same model adopted to simulate steady-state NR and DCM spectra in solution also works for the absorption and vibrational spectra in the matrices, as shown in Fig. 8 for NR and in the ESI† for DCM. We notice that the spectra in solution and in matrices are calculated maintaining constant all molecular model parameters and adjusting the medium relaxation energy ε_{or}. For liquid solvents, the same ε_{or} applies to Raman, absorption and steady-state fluorescence spectra. On the other hand, in matrices, if we use the same ε_{or} as extracted from the absorption and Raman spectra to calculate the steady-state fluorescence spectra, we obtain far too large red shifts. Indeed, in matrices the environmental relaxation is hindered, so that the solvent cannot fully relax before emission takes place. Following a recently proposed approach,[30] steady-state fluorescence spectra can be simulated partitioning the solvent relaxation energy (the one adopted to calculate vibrational and absorption spectra) into a dynamical component, ε_{or}^{dyn}, that describes the degrees of freedom that relax before emission takes place (say 1 ns or so) and a static component, ε_{or}^{st}, that

relaxes on much longer timescales, if ever. This partitioning is somewhat rough, but leads to a simple and effective approach to steady-state fluorescence, as shown in Fig. 8 for NR and in Fig. S11 (ESI†) for DCM.

Our model for time-resolved emission spectra (see the ESI†) can be extended to account for the interaction with the two separate, static and dynamic, components of the reaction field, as generated by the degrees of freedom responsible for the static and dynamic relaxation energy, respectively. But, at variance with liquid solvents, relaxation times for solid matrices are not known: as a matter of fact, our analysis will offer the first reliable information about the relaxation dynamics of the matrices in the 150 fs–15 ns time window. The crude model adopted to describe steady-state emission in solid matrices *via* the partitioning of the relaxation energy into a static and a dynamic component is however too rough to address the complex relaxation phenomena that governs time-resolved emission. Therefore, to simulate the time-resolved emission spectra of NR in mCBPCN and DPEPO we adopt the same model as for liquid solvents (see the ESI†), but introduce a time-dependent relaxation time, to account for the different timescales associated to the different degrees of freedom of the solid matrices.[34] Specifically, we set $\tau_1 = a + b(1 - e^{-ct})$ where a, b and c are adjustable parameters. This function describes an initial relaxation time a that increases in time (with a velocity governed by c) up to the $a + b$ value, representing an environment that, in response to the stimulus related to the molecular excitation, moves initially with velocity $1/a$, and progressively slows down to $1/(a + b)$. The best fit to experimental data are obtained setting a = 20 ps, b = 5 ns and c = 0.001 ps^{-1} for mCBPCN and a = 100 ps, b = 14.9 ns and c = 0.0007 ps^{-1} for DPEPO. An additional adjustment is needed for the mCBPCN matrix, where an initial very fast (<1 ps) relaxation, can only be simulated accounting for an early stage very fast relaxation: for the first 300 fs we consider a relaxation time of 500 fs, which is then switched off. The simulated time-resolved emission spectra in Fig. 9 (*cf.* Fig. 6) compare very well with experimental data, demonstrating that the model is robust and yields reliable information about the dielectric dynamics of amorphous matrices. Similarly, the results in Fig. 7 show an impressive agreement between the experimental and simulated evolution of the emission maxima in the whole accessible time window, 150 fs–15 ns. We notice again that a major discrepancy is observed in the subpicosecond window, where our molecular model, accounting for a single coupled vibrational mode, amplifies coherent oscillations. It is interesting to observe that in mCBPCN some very fast (<1 ps) relaxation occurs, which is most probably related to the vibrational relaxation of CN groups. In any case, even after this early relaxation, our results suggest that, in the accessible time-window, DPEPO is much more sluggish than mCBPCN.

2.5 Discussion

A joint experimental and theoretical study is presented that validates a reliable and effective approach to address the intricate topic of SSS, encompassing a wide range of spectral properties. The most important lesson to be learnt is that, when discussing the dielectric behavior of a medium, the relevant timescale must be specified. Indeed, when looking at static properties (relevant to Raman and absorption spectra), DPEPO is as polar as, or possibly slightly more polar than, DMSO. However, looking at the steady-state fluorescence of NR or DCM, in the timescale of a few nanoseconds, the same matrix looks much less polar.

To rationalize this behavior, we must understand how the environment reacts to the presence of a polar dye. The electronic degrees of freedom of the environment, associated to the medium polarizability, are related to the medium refractive index at optical frequencies.[12,43] Relevant degrees of freedom, typically in the UV region, instantaneously readjust during the excitation of the dye. They are responsible for large effects on the molecular spectral properties when going from the gas phase to an organic medium. However, the marginal variability of the refractive index in common organic media, makes it very difficult to appreciate the role of the environmental electronic polarizability when comparing spectra collected in condensed phases. In other terms, when discussing solvatochromism, *i.e.* the variation of spectral properties of a dye in different environments, the most relevant effect is due to the rearrangement of polar molecules or polar groups around a polar solute. These "orientational" or "polar" degrees of freedom are much slower than the degrees of freedom of the dye, in the visible or IR regions, so that, during the electronic or vibrational excitation of the dye, they are essentially frozen in the configuration equilibrated to the charge distribution of the dye in the ground state.

To measure the static polarity of the environment, polar dyes, like DCM or NR, are good microscopic polarity probes: comparing their absorption or vibrational spectra with those measured in liquid solvents of different polarity, offers a reliable polarity scale. In this perspective, we suggest here a novel and very effective approach relying on Raman spectra. Indeed, getting reliable absorption spectra in matrices is a delicate issue, due to scattering problems, to the tiny absorbance of thin films of diluted samples, and to aggregation phenomena in more concentrated samples. Raman, as a microscopic technique, does not suffer from these problems, and, as an additional bonus, it allows us to check for the matrix homogeneity. We notice that vibrational solvatochromism relies on a subtle effect, often disregarded: the polarizability of the molecular dyes.[47,48] Indeed, upon increasing the solvent polarity, the charge distribution on the dye changes, towards an increased dipole moment. Vibrational frequencies are of course extremely responsive even to small variations of the charge distribution in the molecule, explaining the observed vibrational solvatochromism. If, as in our model, one only accounts for linear electron–vibration coupling, a red-shift of vibrational frequencies of coupled modes and a broadening of corresponding spectral features is expected, in line with the experimental observation.[47,48]

After photoexcitation of a solvatochromic dye (*i.e.* of a dye whose dipole moment changes considerably after excitation), the orientational degrees of freedom of the medium, equilibrated to the ground state charge distribution of the dye, start

to reorganize to respond to the large variation of the charge distribution in the photoexcited dye. Of course, the dynamics of this rearrangement is very different in media of a different nature. In non-viscous liquid solvents, the solvent equilibrates in a few picoseconds,[32] and steady-state fluorescence occurs from a dye surrounded by the solvent equilibrated to the excited state charge distribution.[56,57] This relaxation is responsible for the large Stokes shifts observed for polar molecules in polar solvents. In glassy solvents at cryogenic temperatures, the solvent relaxation is hindered, leading to virtually infinite relaxation times, and the Stokes shifts due to polar solvation vanish, even in highly polar solvents.[33]

The situation is more delicate in solid matrices and SSS, typically discussed with reference to fluorescence spectra,[14–16] and requires a detailed understanding of the dielectric relaxation of the matrix. A careful analysis of the steady-state and time-resolved spectra of two dyes in liquid solvents and amorphous matrices drove us to select NR as a reliable probe for the dielectric relaxation. At variance with DCM, NR is a rigid dye, whose geometry is marginally affected by photoexcitation. Time resolved spectra, collected in both liquid solvents and solid matrices in a very wide time-window, from 15 fs to 15 ns, give us enough information to build and validate a reliable model for the dielectric dynamics in amorphous matrices.

3 Experimental section

3.1 Materials

The two dyes, DCM (4-(dicyanomethylene)-2-methyl-6-(4-dimethylaminostyryl)-4*H*-pyran) and NR, and the four hosts, Zeonex, mCP (1,3-bis(*N*-carbazolyl)benzene), mCBPCN (3,3′-di(carbazol-9-yl)-5-cyano-1,1′-biphenyl) and DPEPO (bis[2-(diphenylphosphino)phenyl]ether oxide), were obtained from commercial suppliers and used as received. Spectrophotometric grade solvents were used without further purification.

3.2 Sample preparation

Solutions. Raman spectra require fairly large dye concentrations to increase the relative intensity of the dye *vs*. the host signal and to improve the signal to noise ratio. The concentration of solutions used for Raman measurements were 2×10^{-3} M in DMSO, 1×10^{-3} in $CHCl_3$ and close to saturation in CCl_4 ($\sim 5 \times 10^{-4}$ M for NR and $\sim 2.5 \times 10^{-4}$ M for DCM). For absorption and fluorescence spectroscopy, solutions with an optical density lower than 0.1 were prepared, corresponding to concentrations $\sim 10^{-6}$ M.

Matrices. Thin films of dye in hosts with different loadings (1%, 0.1% or 0.01% by weight) were prepared either by drop-casting or spin coating. For drop-cast films, 0.1–0.5 mL of solution containing the dye and the host in the required proportion were deposited on a clean quartz substrate and allowed to dry overnight under ambient conditions. Solvents were chosen according to their volatility and to the solubility of the host: films with Zeonex and mCBPCN were drop-cast either from toluene or chloroform, while films with mCP and DPEPO were drop-cast from dichloromethane and chloroform, respectively. Spin-coated films with Zeonex, mCBPCN and DPEPO were prepared from chloroform solution, at a speed of either 1000 rpm or 2200 rpm for 60 s, while mCP films were spin-coated from dichloromethane solution at 1700 rpm for 60 s.

3.3 Raman measurements

Raman spectra were recorded on a Horiba LabRAM HR Evolution Raman microspectrometer equipped with a 785 nm laser. This excitation wavelength compromises between reduced fluorescence background and improved Raman signal. The measurements were performed without moving the grating after instrument calibration to improve wavenumber accuracy. The spectra of the dyes in the different media were obtained by subtracting the spectra of the pure solvents or hosts from the spectra of the solutions or the thin films, recorded under the same conditions. When needed, the fluorescence background was fitted with a polynomial function and subtracted.

Solutions were placed in quartz cells with a 1 cm path length, using a 10× magnification objective and focusing the laser beam 3 mm below the cell surface. For films, a 100× magnification objective was used. The independence of the spectra on dye concentration was checked both in solution and thin films to exclude aggregation effects.

3.4 Absorption, fluorescence spectra and TRES

Absorption spectra were collected with a PerkinElmer Lambda 650 double-beam spectrophotometer. Fluorescence measurements were performed with a FLS1000 Edinburgh Instruments fluorometer equipped with a Xe lamp as the excitation source for steady-state measurements and with an EPL-405 (Edinburgh Instruments) picosecond pulsed laser diode (wavelength: 405 nm) for time-resolved measurements. Time-resolved emission spectra (TRES) were recorded with the time-correlated single-photon counting (TCSPC) technique, using the same experimental setup. The temporal evolution of TRES was analyzed using a global analysis approach (see the ESI†).

3.5 Pump–probe experiments

Pump–probe measurements have been performed on two experimental setups with different time resolutions and different maximum delay times; they will be labeled as ''Long Range pump–probe'' (LR-pp) and ''Ultrashort pump–probe'' (US-pp). The output of a Coherent Legend Elite USP regen amplifier (1 KHz, 800 nm, 40 fs, 3.5 mJ) is redistributed with the help of a series of broadband beam-splitters using the following scheme.

850 μJ of the 800 nm source are used for the LR-pp setup. The main beam, after passing through a fused-silica wedge plate, is used to pump an Optical Parametric Amplifier (TOPAS, LightConversion) to generate signal (1200–1600 nm) and idler (1600–2300 nm) pulses. The signal pulse is then combined with the residual 800 nm pulse in a BBO sum frequency generation crystal to produce the pump pulses (0.5–4 μJ) tunable in the 480–525 nm spectral range. The reflection coming from the wedge plate is sent to a computer controllable delay line and then focused on a 2 mm CaF2 Window to generate

supercontinuum (spectral range 350–750 nm). Supercontinuum is further split into two pulses, using a 50% beam-splitter, to generate probe and reference pulses. The probe and reference are then focused and spatially overlapped with the pump pulse on the sample, thanks to a 100 EFL spherical mirror. The delay time between the pump and probe is continuously adjusted, using the optical delay line mentioned before (bidirectional position reproducibility better than 25 fs, while the maximum available delay time is 1.5 ns). The optical path of the reference is constructed in such a way that it is always the first pulse interacting with the sample, always before the pump and probe. The probe and reference are then focused on the entrance of a spectrograph (Jobin-Yvon CP140) and dispersed on two separate arrays (256 pxs, Hamamatsu). Pump pulses are alternatively blocked/unblocked before the sample by an optical chopper (Thorlabs, frequency repetition rate ~70 Hz). The transient absorption spectrum is finally obtained as: $\Delta\mathrm{Abs}(\lambda,t) = -\log((I^{\mathrm{on}}_{\mathrm{probe}}/I^{\mathrm{on}}_{\mathrm{ref}}) \times (I^{\mathrm{off}}_{\mathrm{ref}}/I^{\mathrm{off}}_{\mathrm{probe}}))$.

For the (US-pp) setup we use 450 μJ of the 800 nm source. For Ultrashort pump–probe (US-pp) measurements, a modified version of the setup for two-dimensional visible spectroscopy described in ref. 58, is used. Briefly, ultrafast pulses coming from the Coherent Legend Elite USP are sent to two Non-Collinear Optical Parametric Amplifiers (NOPAs) that generate chirped pulses (max output 2 μJ energy per pulse) tunable between 500 and 780 nm with an asymmetric shape and full width at half maximum ~80–90 nm (NOPA-a) and 110–120 nm (NOPA-b). The pulses are then compressed by a couple of chirped mirrors (DCM10 Venteon): after a total of 9 bounces the dispersion introduced by the optics is very well compensated at the sample region, in such a way that the duration retrieved by PG-FROG analysis is around 12 fs. The output of NOPA-b is then split in two pulses, by a 50% beam-splitter, to generate the probe and reference pulses. The output of NOPA-a is used as the pump pulse, while the output of NOPA-b is used as a probe. After dispersion compensation, pump pulses follow the scheme described in ref. 58 to generate two collinear pump pulses for 2D spectroscopy. Blocking one of the two pulses, it is possible to acquire pump–probe spectra. The pump pulse is sent to an optical delay line (Physik-Instrumente, bidirectional reproducibility better that 5 femtoseconds and maximum delay ~250 picoseconds) to control the delay vs the probe pulses. Pump, probe and reference beams are focused on the sample using a spherical mirror with 250 mm EFL, but only the pump and probe are spatially overlapped on the sample. After the sample, the pump is blocked by a beam-stopper while the probe and reference are focused on the entrance of a spectrograph (Jobin-Yvon CP140) and dispersed on two separate arrays (256 pxs, Hamamatsu). The probe and reference intensities are acquired and the transient absorption spectra are finally calculated as described before.

4 Conclusions

Understanding how optical properties of an organic dye are affected when the dye is dispersed in a matrix is crucial for the optimization of materials for OPVs, OLEDs, organic solar concentrators and the like. However, while solvatochromism, *i.e.* the dependence of optical spectra of organic dyes on the local environment, is well recognized in low viscosity solvents, SSS is still far less understood. Here we present an extensive experimental and theoretical study of SSS that exploits two commercial solvatochromic dyes to characterize the static and dynamic dielectric response of several amorphous matrices of interest for OLED applications. The most important result is that in SSS one has to be careful to distinguish between the dielectric properties that define the spectral responses of the dye at equilibrium, *i.e.* absorption and Raman spectra, and those related to emission spectra, occurring from an out of equilibrium state. In the first case, the dynamical behavior of the matrix is irrelevant, while for emission spectra, the dielectric dynamics of the matrix is of paramount importance. We mention that in liquid solvents the dielectric relaxation is completed in a few picoseconds, so that steady-state emission occurs from the fully relaxed system and the study of solvent relaxation requires ultrafast spectroscopic measurement.

We propose a simple and reliable approach to estimate the matrix dielectric properties relevant to equilibrium spectral responses exploiting vibrational solvatochromism. Micro-Raman measurements on DCM and NR dyes dispersed in solid matrices can be compared with the corresponding spectra collected in solvents with known polarity to define a polarity scale. We demonstrated that the non-polar Zeonex matrix has similar Raman spectra as CCl_4, mCP and mCBPCN have similar polarity to DMSO and DPEPO is slightly more polar. The frequency of the steady-state fluorescence spectra instead depends in an intricate way on the matrix polarity and on its dynamics. Good molecular probes of local polarity for dynamical studies must be selected as solvatochromic dyes with a rigid structure, so that the relaxation of the molecular conformational degrees of freedom does not interfere with the matrix dynamics. We selected for this aim NR and recorded its time-resolved emission spectra in a wide time window, ranging from 15 fs to 15 ns, comparing the results in liquid solvents and matrices. A detailed microscopic model is first parametrized and validated against steady-state spectra. The same model is extended to address time-resolved emission in a liquid solvent, where literature data about solvent relaxation time allow us to validate our approach to time-resolved emission spectra without the need for additional fitting parameters. On this solid basis, the simulation of time-resolved spectra of NR in two polar matrices gives the first reliable estimate of relevant relaxation times. Indeed, a single relaxation time is not enough to describe the matrix relaxation, and a time-dependent relaxation time must be introduced. In any case, our results point to a sluggish relaxation of DPEPO if compared with mCBPCN. Our data, supported by a detailed theoretical model, definitely demonstrate that the dielectric relaxation in polar amorphous matrices is not fully frozen and definitely occurs on timescales that extend beyond 10 ns.

Author contributions

Bardi and Sissa: sample preparation and data acquisition; Giavazzi, Di Maiolo, and Phan Huu: theoretical analysis; Ferrari

and Masino: Raman experiments; Lapini, Di Donato, and Iagatti: pump–probe experiments; Painelli: conceptualization. All: methodology, writing and review.

Conflicts of interest

There are no conflicts to declare.

Acknowledgements

Work in Parma was funded by the PNRR MUR project ECS-00000033-ECOSISTER and benefited from the local HPC center and from the equipment and framework of the COMP-HUB and COMP-R Initiatives, funded by the 'Departments of Excellence program of the Italian Ministry for University and Research' (MIUR, 2018–2022 and MUR, 2023–2027). Work in Florence was supported by the EU Horizon 2020 research and innovation program under grant agreement 871124 Laserlab-Europe. F. D. M.'s position was co-funded by the European Union – PON Research and Innovation 2014–2020. A. L. acknowledges support from the Fondazione Cassa di Risparmio di Torino (CRT), Visco3DCell project and from the University of Parma, MUR-DM737-2022-FIL-PROGETTI-A-LAPINI project.

Notes and references

1 O. Ostroverkhova, *Chem. Rev.*, 2016, **116**, 13279–13412.
2 F. Biscarini, E. Coronado, A. Painelli and M. Yamashita, *J. Mater. Chem. C*, 2021, **9**, 10521–10523.
3 W. Liptay, *Angew. Chem., Int. Ed. Engl.*, 1969, **8**, 177–188.
4 C. Reichardt, *Chem. Rev.*, 1994, **94**, 2319–2358.
5 S. Di Bella, T. J. Marks and M. A. Ratner, *J. Am. Chem. Soc.*, 1994, **116**, 4440–4445.
6 J. R. Lakowicz, *Principles of Fluorescence Spectroscopy*, Springer, US, 1999, p. 698.
7 J. Tomasi, B. Mennucci and R. Cammi, *Chem. Rev.*, 2005, **105**, 2999–3094.
8 B. Lunkenheimer and A. Köhn, *J. Chem. Theory Comput.*, 2013, **9**, 977–994.
9 J. A. Bjorgaard, V. Kuzmenko, K. A. Velizhanin and S. Tretiak, *J. Chem. Phys.*, 2015, **142**, 044103.
10 C. A. Guido and S. Caprasecca, *Int. J. Quantum Chem.*, 2019, **119**, e25711.
11 T. Vreven and K. Morokuma, *Hybrid Methods: ONIOM(QM:MM) and QM/MM*, Elsevier, 2006, ch. 3, vol. 2, pp.35–51.
12 D. K. A. Phan Huu, R. Dhali, C. Pieroni, F. Di Maiolo, C. Sissa, F. Terenziani and A. Painelli, *Phys. Rev. Lett.*, 2020, **124**, 107401.
13 R. Dhali, D. K. A. Phan Huu, F. Terenziani, C. Sissa and A. Painelli, *J. Chem. Phys.*, 2021, **154**, 134112.
14 V. Bulović, A. Shoustikov, M. Baldo, E. Bose, V. Kozlov, M. Thompson and S. Forrest, *Chem. Phys. Lett.*, 1998, **287**, 455–460.
15 V. Bulović, R. Deshpande, M. Thompson and S. Forrest, *Chem. Phys. Lett.*, 1999, **308**, 317–322.
16 A. P. Green, K. T. Butler and A. R. Buckley, *Appl. Phys. Lett.*, 2013, **102**, 133501.
17 S. Y. Leblebici, T. L. Chen, P. Olalde-Velasco, W. Yang and B. Ma, *ACS Appl. Mater. Interfaces*, 2013, **5**, 10105–10110.
18 S. Torabi, F. Jahani, I. V. Severen, C. Kanimozhi, S. Patil, R. W. A. Havenith, R. C. Chiechi, L. Lutsen, D. J. M. Vanderzande, T. J. Cleij, J. C. Hummelen and L. J. A. Koster, *Adv. Funct. Mater.*, 2014, **25**, 150–157.
19 X. Liu, B. Xie, C. Duan, Z. Wang, B. Fan, K. Zhang, B. Lin, F. J. M. Colberts, W. Ma, R. A. J. Janssen, F. Huang and Y. Cao, *J. Mater. Chem. A*, 2018, **6**, 395–403.
20 S. Sami, R. Alessandri, R. Broer and R. W. A. Havenith, *ACS Appl. Mater. Interfaces*, 2020, **12**, 17783–17789.
21 G. Méhes, K. Goushi, W. J. Potscavage and C. Adachi, *Org. Electron.*, 2014, **15**, 2027–2037.
22 F. B. Dias, J. Santos, D. R. Graves, P. Data, R. S. Nobuyasu, M. A. Fox, A. S. Batsanov, T. Palmeira, M. N. Berberan-Santos, M. R. Bryce and A. P. Monkman, *Adv. Sci.*, 2016, **3**, 1600080.
23 M. K. Etherington, J. Gibson, H. F. Higginbotham, T. J. Penfold and A. P. Monkman, *Nat. Commun.*, 2016, **7**, 13680.
24 P. K. Samanta, D. Kim, V. Coropceanu and J.-L. Brédas, *J. Am. Chem. Soc.*, 2017, **139**, 4042–4051.
25 J.-M. Mewes, *Phys. Chem. Chem. Phys.*, 2018, **20**, 12454–12469.
26 D. K. A. Phan Huu, S. Saseendran and A. Painelli, *J. Mater. Chem. C*, 2022, **10**, 4620–4628.
27 A. J. Gillett, A. Pershin, R. Pandya, S. Feldmann, A. J. Sneyd, A. M. Alvertis, E. W. Evans, T. H. Thomas, L.-S. Cui, B. H. Drummond, G. D. Scholes, Y. Olivier, A. Rao, R. H. Friend and D. Beljonne, *Nat. Mater.*, 2022, **21**, 1150–1157.
28 P. L. dos Santos, J. S. Ward, M. R. Bryce and A. P. Monkman, *J. Phys. Chem. Lett.*, 2016, **7**, 3341–3346.
29 T. Serevičius, R. Skaisgiris, J. Dodonova, I. Fiodorova, K. Genevičius, S. Tumkevičius, K. Kazlauskas and S. Juršenas, *J. Phys. Chem. Lett.*, 2022, **13**, 1839–1844.
30 D. K. A. Phan Huu, S. Saseendran, R. Dhali, L. G. Franca, K. Stavrou, A. Monkman and A. Painelli, *J. Am. Chem. Soc.*, 2022, **144**, 15211–15222.
31 E. W. Castner, M. Maroncelli and G. R. Fleming, *J. Chem. Phys.*, 1987, **86**, 1090–1097.
32 M. L. Horng, J. A. Gardecki, A. Papazyan and M. Maroncelli, *J. Phys. Chem.*, 1995, **99**, 17311–17337.
33 C. Sissa, A. Painelli, M. Blanchard-Desce and F. Terenziani, *J. Phys. Chem. B*, 2011, **115**, 7009–7020.
34 Z. Ahmad, *Dielectric Material*, InTech, 2012.
35 T. Northey, J. Stacey and T. J. Penfold, *J. Mater. Chem. C*, 2017, **5**, 11001–11009.
36 C. Deng, L. Zhang, D. Wang, T. Tsuboi and Q. Zhang, *Adv. Opt. Mater.*, 2019, **7**, 1801644.
37 C. F. Madigan and V. Bulović, *Phys. Rev. Lett.*, 2003, **91**, 247403.
38 B. L. Cotts, D. G. McCarthy, R. Noriega, S. B. Penwell, M. Delor, D. D. Devore, S. Mukhopadhyay, T. S. D. Vries and N. S. Ginsberg, *ACS Energy Lett.*, 2017, **2**, 1526–1533.
39 X. de Vries and R. Coehoorn, *Phys. Rev. Mater.*, 2020, **4**, 085602.

40 Y. Olivier, B. Yurash, L. Muccioli, G. D'Avino, O. Mikhnenko, J. C. Sancho-García, C. Adachi, T.-Q. Nguyen and D. Beljonne, *Phys. Rev. Mater.*, 2017, **1**, 075602.
41 B. Boldrini, E. Cavalli, A. Painelli and F. Terenziani, *J. Phys. Chem. A*, 2002, **106**, 6286–6294.
42 F. Terenziani and A. Painelli, *Phys. Chem. Chem. Phys.*, 2015, **17**, 13074–13081.
43 A. Painelli, *Chem. Phys.*, 1999, **245**, 185–197.
44 R. Dhali, D. K. A. Phan Huu, F. Bertocchi, C. Sissa, F. Terenziani and A. Painelli, *Phys. Chem. Chem. Phys.*, 2021, **23**, 378–387.
45 Y. Wada, K. Shizu and H. Kaji, *J. Phys. Chem. A*, 2021, **125**, 4534–4539.
46 J. B. Weaver, J. Kozuch, J. M. Kirsh and S. G. Boxer, *J. Am. Chem. Soc.*, 2022, **144**, 7562–7567.
47 F. Terenziani, A. Painelli and D. Comoretto, *J. Phys. Chem. A*, 2000, **104**, 11049–11054.
48 A. Painelli and F. Terenziani, *J. Phys. Chem. A*, 2000, **104**, 11041–11048.
49 A. Painelli and F. Terenziani, *Synth. Met.*, 2001, **116**, 135–138.
50 E. Crovini, R. Dhali, D. Sun, T. Matulaitis, T. Comerford, A. Slawin, C. Sissa, F. Azzolin, F. Di Maiolo, A. Painelli and E. Zysman-Colman, *J. Mater. Chem. C*, 2023, **11**, 8284–8292.
51 F. Terenziani, A. Painelli, A. Girlando and R. M. Metzger, *J. Phys. Chem. B*, 2004, **108**, 10743–10750.
52 S. Sanyal, C. Sissa, F. Terenziani, S. K. Pati and A. Painelli, *Phys. Chem. Chem. Phys.*, 2017, **19**, 24979–24984.
53 F. Di Maiolo and A. Painelli, *Phys. Chem. Chem. Phys.*, 2020, **22**, 1061–1068.
54 D. Giavazzi, F. Di Maiolo and A. Painelli, *Phys. Chem. Chem. Phys.*, 2022, **24**, 5555–5563.
55 D. Giavazzi, S. Saseendran, F. Di Maiolo and A. Painelli, *J. Chem. Theory Comput.*, 2022, **19**, 436–447.
56 F. Terenziani and A. Painelli, *Chem. Phys.*, 2003, **295**, 35–46.
57 A. Painelli and F. Terenziani, *Chem. Phys. Lett.*, 1999, **312**, 211–220.
58 S. Doria, M. Di Donato, R. Borrelli, M. F. Gelin, J. Caram, M. Pagliai, P. Foggi and A. Lapini, *J. Mater. Chem. C*, 2022, **10**, 7216–7226.